REDUCED GRAVITY COMBUSTION OF THERMOPLASTIC SPHERES

by

Jiann C. Yang, Anthony Hamins, and Michelle K. Donnelly
Building and Fire Research Laboratory
National Institute of Standards and Technology
Gaithersburg, MD 20899 USA

Reprinted from Combustion and Flame, Vol. 120, Nos. 1/2, 61-74, January 2000

NIST
National Institute of Standards and Technology
Technology Administration, U.S. Department of Commerce

Reduced Gravity Combustion of Thermoplastic Spheres

JIANN C. YANG*, ANTHONY HAMINS, AND MICHELLE K. DONNELLY
Building and Fire Research Laboratory, National Institute of Standards and Technology, Gaithersburg, MD 20899, USA

A series of low-gravity experiments were conducted to investigate the combustion of supported thermoplastic polymer spheres under varying ambient conditions. The three types of thermoplastic investigated were polymethylmethacrylate (PMMA), polypropylene (PP), and polystyrene (PS). The low-gravity environment was achieved by performing the experiments aboard the NASA DC-9 and the KC-135 Reduced Gravity Aircraft. Spheres with diameters ranging from 2 mm to 6.35 mm were tested yielding Grashof numbers calculated to be less than 0.1. The polymer sphere was supported using a 75-μm-diameter Al/Cr/Fe alloy wire. The total initial pressure varied from 0.05 MPa to 0.15 MPa whereas the ambient oxygen concentration varied from 19% to 30% (by volume). The ignition system consisted of a pair of retractable energized coils. Two CCD cameras recorded the burning histories of the spheres. The video sequences revealed a number of dynamic events including bubbling, and sputtering as well as soot shell formation and break-up during combustion of the spheres at reduced gravity. The ejection of combusting material from the burning spheres represents a fire hazard that must be considered at reduced gravity. The ejection was found to be sensitive to polymer type, but independent of oxygen concentration and pressure. The average value of the ejection frequency was found to be 3 Hz, 5 Hz, and 5 Hz for PMMA, PS, and PP, respectively. The velocities of the ejected material were estimated by tracking the material in two consecutive video frames. For the PP spheres, V_a = 2.3 ($\pm$ 1.2) cm/s (with 60 events observed). The ejected material appeared to decelerate at an average rate of $\approx$ 40 cm/s^2, and traverse an average distance of only 8 mm before burning to completion. The V_a for PS and PMMA was not determined because the ejected material was never observed to exist beyond the visible flame of the parent sphere.

The average mass burning rates were measured to increase with initial sphere diameter and oxygen concentration, whereas the initial pressure had little effect. The three thermoplastic types exhibited different burning characteristics. For the same initial conditions, the mass burning rate of PP was slower than PMMA, whereas the mass burning rate of PS was comparable to PMMA. The transient diameter of the burning thermoplastic exhibited two distinct periods: an initial period (enduring approximately half of the total burn duration) when the diameter remained approximately constant, and a final period when the square of the diameter linearly decreased with time. A simple homogeneous two-phase model was developed to understand the changing diameter of the burning sphere. Its value is based on a competition between diameter reduction due to mass loss from burning and sputtering, and diameter expansion due to the processes of swelling (density decrease with heating) and bubble growth. The model relies on empirical parameters for input, such as the burning rate and the duration of the initial and final burning periods. Published by Elsevier Science Inc.

INTRODUCTION

With the advent of space exploration, fire safety aboard space vehicles including space capsules, the Space Shuttle, and the permanent space station presents new challenges. An ideal way to alleviate a portion of the fire hazard is to eliminate completely the use of flammable materials or to replace them with low-flammability, fire-retarded materials. Such an approach, however, is not practical in the near future. Materials (e.g., paper and plastics) that are flammable under certain conditions will surely be employed, posing a potential threat to the safety of crew and spacecraft. Therefore, an understanding of the combustion characteristics of such materials under different ambient conditions and in a reduced gravity environment is of interest.

Polymer combustion is a highly complicated process where chemical reactions may occur not only in the gas phase, but also in the condensed phase, as well as at the solid–gas interface [1]. The chemistry depends strongly on the coupling between the condensed-phase and gas-phase phenomena. For some polymers, additional complications arise due to the formation of char layers. For others, the behavior of the condensed phase involves swelling, bubbling, melt-

*Corresponding author. E-mail: jiann.yang@nist.gov

COMBUSTION AND FLAME 120:61–74 (2000)
Published by Elsevier Science Inc.
0010-2180/00/$–see front matter
PII S0010-2180(99)00084-X

ing, sputtering, in-depth pyrolysis, and multi-stage combustion [1–4]. Some of these features bear a resemblance to phenomena observed in coal particle combustion [5]. In addition to its relevance to spacecraft fire safety, the combustion of polymeric materials is related to other applications including solid and hybrid rocket propulsion, and of recent interest, waste incineration [6–12].

The mass burning rate is a key parameter in the characterization of polymer combustion. It is directly related to heat release and thereby, fire hazard. The mass burning rate is often used to rank polymer flammability and to evaluate the inhibition of polymer flammability by additives that act as flame retardants [13].

Most of the experimental observations reported in this paper have been obtained for poly-methylmethacrylate (PMMA), which was chosen because of its well-characterized thermophysical properties. Furthermore, the combustion of PMMA is unique in that it is a noncharring thermoplastic, which simplifies an analysis of the experimental data. Although the combustion of PMMA has been extensively studied in normal gravity experiments, only a limited amount of work has been conducted in reduced gravity [14–17]. In addition to using PMMA spheres, several limited sets of experiments have also been performed using two other thermoplastics, polypropylene (PP) and polystyrene (PS), in order to examine the effects of material properties on burning characteristics at reduced gravity.

A spherical geometry for the sample was used in this study because it represents the simplest possible combustion configuration in reduced gravity, namely a one-dimensional flame system. In addition, a burning thermoplastic sphere is expected to be analogous to the combustion of a liquid fuel droplet [2–4, 8, 9], a well-developed field of study [18]. Some differences with liquid fuel droplet combustion can also be expected due to the complex condensed-phase processes occurring during combustion. Although several studies on the combustion of thermoplastic spheres at normal gravity have been cited [2–4, 8, 9], only recently have reduced gravity experiments been reported [19–22]. The difficulty in conducting polymer sphere combustion experiments in normal gravity is that the spherical geometry of the sample is not maintained once dripping of the polymer melt begins. The main objective of the present work is to examine experimentally the combustion characteristics of the three aforementioned thermoplastics and to obtain their burning rates in low gravity under different ambient oxygen concentrations, X_O, (19.9% to 30% by volume) and total pressures (0.5 MPa to 0.15 MPa). It is anticipated that the simple spherical geometry in conjunction with reduced gravity conditions will facilitate an assessment of the effect of condensed-phase behavior on the polymer burning processes and that the measurements can be used as a means to validate polymer combustion models [e.g., 23, 24].

EXPERIMENTAL APPARATUS

A reduced gravity environment was achieved by performing experiments aboard the NASA DC-9 and the KC-135 Reduced Gravity Aircraft. The time available to carry out the experiments in both the 2.2-s and 5.18-s NASA drop towers is not long enough to observe the complete burning history for even moderate sized polymer spheres (initial diameters greater than 3 mm). Thus, experiments were performed onboard the Reduced Gravity Aircraft, although the quality of the low-gravity environment in a drop tower (less than 10^{-4} G; G being the gravitational acceleration at sea level) is considerably superior to an aircraft flying a parabolic trajectory ($\approx 10^{-2}$ G). For all of the reduced gravity experiments, the Grashof number was estimated to be less than 0.1.

The experimental hardware was housed inside a rack (60 cm × 60 cm × 106 cm). The hardware consisted of a laptop computer, a data acquisition and control system used for storing gravity-level information during the experiments and for controlling a pair of micro-step controllers and linear motors (and associated ignition system), a combustion chamber, power supplies, two Hi8 mm CCD cameras, two ignition systems, and a vacuum pump. Oxygen/nitrogen mixture cylinders were mounted separately in a gas bottle rack. The combustion chamber was cylindrical, 50 cm long and 25 cm diameter, large enough such that changes in

TABLE 1

Experimental Test Matrix

Material	Initial Sphere Diameter (D_o, mm)	Oxygen Mole Percent (X_O)	Total Pressure (MPa)
PMMA	2.0, 2.5, 3.0, 3.2, 4.8, 6.4	19.9, 21.0, 25.0, 30.0	0.05, 0.10, 0.15
PP	2.4, 3.0	21.0, 25.0, 30.0	0.05, 0.10
PS	3.0	25.0	0.05

chamber pressure and oxygen content were minimal during combustion of the thermoplastic sphere. The vacuum pump was used to evacuate the combustion products and facilitate the flushing and filling of the combustion chamber with the desired oxygen/nitrogen mixtures in the normal gravity tests. For the reduced gravity experiments, the overboard vent of the aircraft was used for operational convenience. A detailed description of the experimental package is given in [20].

The polymer spheres were burned in a suspended configuration. Several techniques for fabricating a suspended sphere were attempted [19]. The procedure and hardware used to obtain the suspended sphere have been described in detail elsewhere [19, 20]. A 75-μm-diameter Al/Cr/Fe alloy wire was stretched and heated locally by resistive heating. The sphere was placed on a three-dimensional translation stage and positioned toward the heated portion of the wire. As the sphere touched the heated wire, part of it softened, such that the wire could be easily inserted into the thermoplastic sphere. Local heating of the sphere during the process of embedding the wire can alter the shape of the sphere slightly, but the changes were insignificant if the electric current through the wire was carefully controlled. The supported polymer sample was mounted at the center of a removable holder, which was inserted along two parallel tracks on the combustion chamber wall.

Several ignition methods were investigated [19, 20]. The ignition technique employed in this study used a pair of small heating coils made of metal alloy wire, with a diameter of 250 μm. The coil was formed by wrapping the wire around a 1-mm-diameter screw, yielding a cylindrically shaped coil, approximately 3 mm long and 1.5 mm in diameter. The coils were mounted on independent, computer-controlled motorized linear translation tracks, positioned symmetrically on opposite sides of the thermoplastic sphere. The coils were oriented with the long axis of the coil perpendicular to the linear track. To ignite a thermoplastic sphere, the coils were resistively heated using a filament transformer. The power to the coils was maintained for a fixed duration (5.5 s) for all experiments, ensuring uniformity of the ignition event. The energized coils were moved toward the sample surface until contact was just made. After contact for 2 s, the coils were slowly ($\approx$ 0.5 cm/s) retracted. Ignition was typically observed 1 s to 2 s after the coil made contact with the sphere, depending on ambient conditions.

The heat flux from the coil was characterized using a small cylindrical Schmidt-Boelter gauge with a flat 6-mm-diameter face and a flat spectral response. The coil was positioned to just touch the front of the gauge and the output of the gauge was recorded as the coil was energized. The measurements showed that the flux duration was approximately 6 s, with the average and maximum flux during the 2 s contact period equal to $\approx$ 340 kW/m^2 and $\approx$ 380 kW/m^2, respectively.

Table 1 summarizes the experimental conditions. The sphere diameters were selected based on commercial availability and were limited to small diameters (less than 6 mm), to assure near-complete burning during the available duration of reduced gravity. Since pressure effects have been observed in the burning rate of liquid droplets, the effect of pressure was considered [25, 26]; however, safety constraints for the combustion chamber governed the upper pressure limit (0.15 MPa) for the experiments, whereas the lower pressure limit (0.05 MPa) was selected to ensure successful ignition of the spheres.

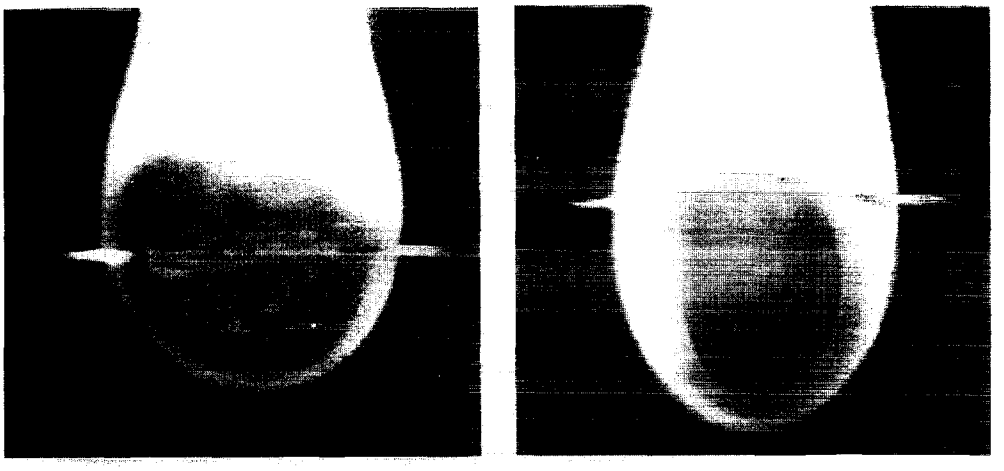

(a) (b)

Fig. 1. Video images showing a PMMA sphere burning at normal gravity (D_o = 4.76 mm, 0.10 MPa, and 25% O_2), before (a) and after (b) the occurrence of dripping of the polymer melt.

RESULTS AND DISCUSSION

Observations of the suspended sphere experiments in normal gravity can be summarized qualitatively as follows. Upon ignition, the sphere softened and swelled, and internal bubbling occurred. The violent ejection of molten material was not observed. The sphere shape deformed due to the action of gravity on the polymer melt, followed by dripping of the molten thermoplastic. Depending on the type of thermoplastic, the flames varied in luminosity and smoke. Finally, the deformed burning sphere fell off the suspension wire. This occurred in less than 10 s after ignition for all sphere diameters used in this study and it was not possible to observe complete burning of the samples, making average burning rate measurements impractical. Figure 1 shows two images selected from the video recording of a PMMA sphere burning at normal gravity before and after the initiation of dripping of the polymer melt. The shape of the sample was significantly distorted from that of a sphere, due to the influence of gravity as dripping occurred.

The period of reduced gravity provided by the NASA DC-9 and the KC-135 Reduced Gravity Aircraft was not long enough to obtain complete burning histories of spheres with initial diameters (D_o) greater than 3 mm for the range of conditions tested. For these large spheres (D_o > 3 mm), the diameter of the burning spheres did not appear to change significantly during the reduced gravity period. The mass loss due to burning was presumably balanced by increases in the apparent sphere diameter due to bubbling and swelling. For smaller spheres (D_o < 3 mm), complete combustion was observed. Flame extinction, a phenomenon frequently observed in liquid droplet microgravity combustion, was not observed in any of the sphere burning experiments.

Under reduced gravity conditions, experimental observations of the suspended PMMA spheres revealed a very different burning character. Figure 2 is a representative video sequence showing a 3-mm-diameter PMMA sphere before and after ignition during reduced gravity. In Fig. 2, the components of the gravity vector (Gz, Gx, and Gy) are displayed at the bottom of each frame, while the date, time, and the parabolic trajectory number are displayed at the top of each frame. The sphere appeared to move randomly with respect to the suspension wire during combustion. The glowing ignition coil is seen in the first frame of the sequence. Ignition occurred approximately 3 s after the first frame and 2 s before the second. As the coil was retracted, it was de-energized and became less luminous. Upon ignition, the sample swelled and the outermost surface layer of the burning sample bubbled. A spherical blue flame was often observed, with its duration decreasing with total ambient pressure and oxygen concentration. The spherical flame subsequently became more luminous (yellowish in color), more bubbles nucleated, internal bubbling intensified, and a soot shell formed between the outer

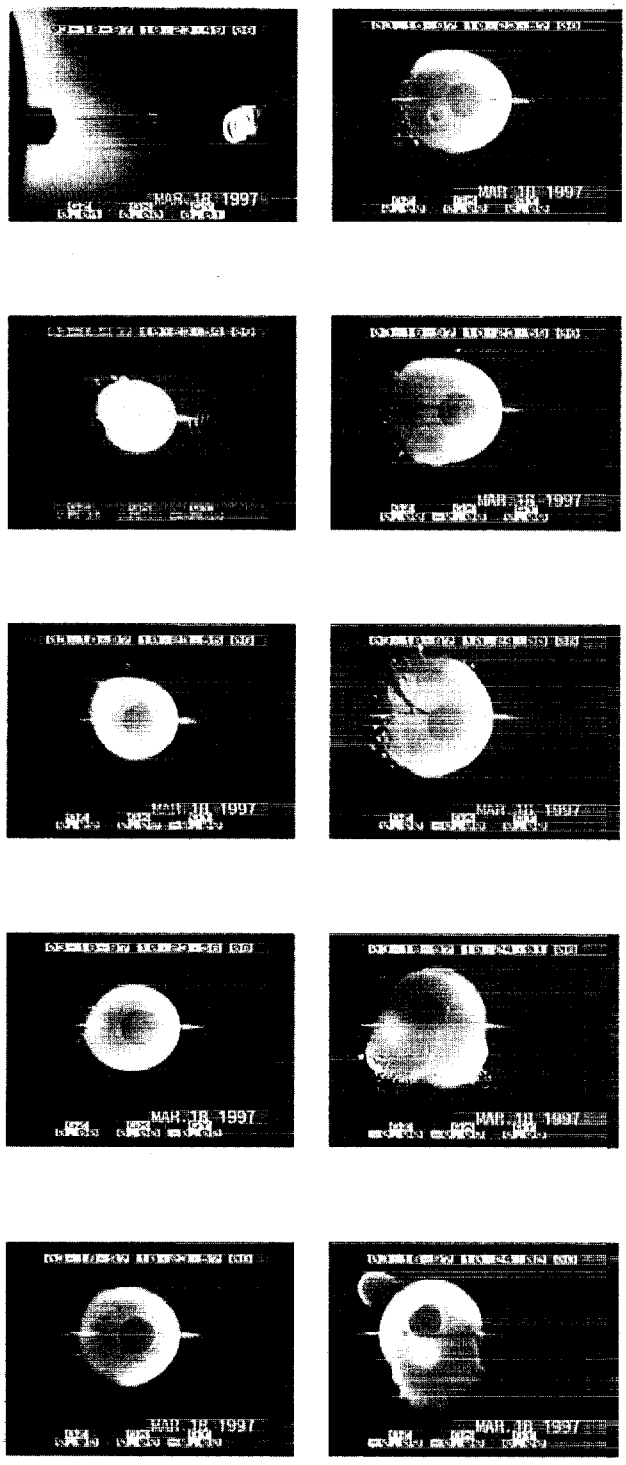

Fig. 2. A video sequence (from top to bottom, and left to right) showing a PMMA sphere before and after ignition under reduced gravity conditions (D_o = 3 mm, 0.15 MPa, and 30% O_2); also shown is the energized-wire ignition device.

luminous flame and the thermoplastic sphere. Sputtering and ejection of molten polymer from the burning sphere were observed, followed by break-up of the soot shell. The internal bubbling

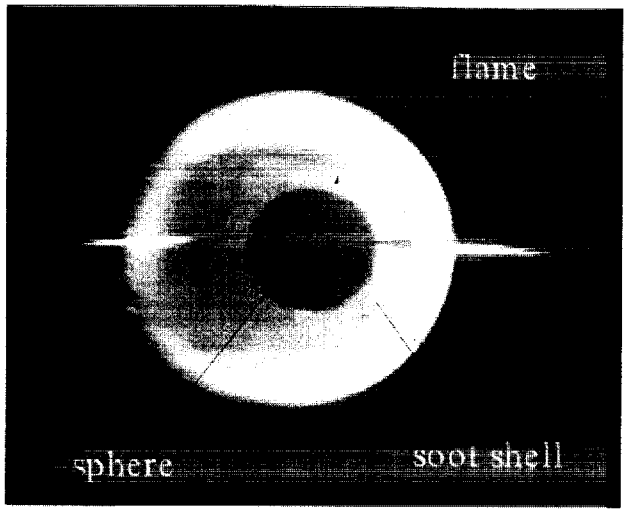

Fig. 3. Break-up of a soot shell from a burning PMMA sphere under reduced gravity conditions (D_o = 3 mm, 0.15 MPa, and 30% O_2).

and ejection of material imparted momentum to the suspended sphere, causing it to exhibit impulsive motion and to slide along the support wire after melting had occurred through the sphere interior. The flame then lost its spherical shape, probably due to the motion of the sphere. The movement of the sample appeared to be more severe for spheres with a small initial diameter, possibly because of their smaller inertia and/or because of the rapid propagation of the molten front through the sphere. Although the ejection process temporarily perturbed the shape of the thermoplastic sphere in reduced gravity, the spherical shape tended to be restored. This was particularly true towards completion of fuel burning when the sphere diameter was small (small Grashof number), and motion of the suspended sphere was reduced (possibly due to surface tension effects).

Figure 3 is an enlarged video image of a burning PMMA sphere showing the break-up of a soot shell located between the luminous flame zone and the sphere surface. The formation of a soot shell is not surprising because the main PMMA degradation product is methylmethacrylate [27], which has a sooting character similar to that of heptane (exemplified by their nearly equal smoke heights [28]), and soot shells have been observed during the combustion of heptane droplets at reduced gravity [29–31]. The break-up of the soot shell in the figure is reminiscent of the phenomena associated with a

toluene droplet burning at reduced gravity with a small drift velocity [32].

Although bubbling was observed during combustion in normal gravity, the ejection of molten material was not observed. Gravity-induced dripping of the melt appears to counteract the material ejection process because the transport of bubbles to the sphere surface is resisted by the downward flow of the polymer melt. In terms of microgravity fire safety, the ejected burning material poses a potential ignition hazard to nearby flammable objects.

Figures 4 and 5 are representative video sequences showing burning 3-mm-diameter polypropylene (PP) and polystyrene (PS) spheres, respectively, before and after ignition during parabolic flights. The combustion of PP and PS generally resembled that of PMMA; however, some salient differences were observed. A blue flame, observed immediately after ignition of PMMA, was not observed in the PP or PS flames. For PP, small burning particles were ejected through the flame from the parent sphere during combustion (see discussion below). There was less vibrating and sliding motion of the PP spheres along the wire than for the PMMA. The burning PS suspended sphere moved frequently with respect to the support wire. The flames were highly luminous. The spheres are not visible in Fig. 5 because of the intense flame luminosity, which suggests the presence of large quantities of soot particles, similar to that observed in normal gravity burning of PS.

The video record suggests that the dynamic ejection events bear some resemblance to the phenomena of bursting of single bubbles at a gas/liquid interface, which has been described by Tomaides and Whitby [33]. It appears that two different dynamic ejection events play a role in the burning of a thermoplastic in microgravity. The first type, which was observed during the combustion of the three thermoplastics, is a luminous flame protrusion attached to the parent flame surrounding the sphere. This may be due to the release of gas jets associated with bubble bursting [33]. The second type, which was observed during PP combustion only, is the infrequent ejection of burning material that is transported through the flame and beyond for some distance. This may be due to the ejection

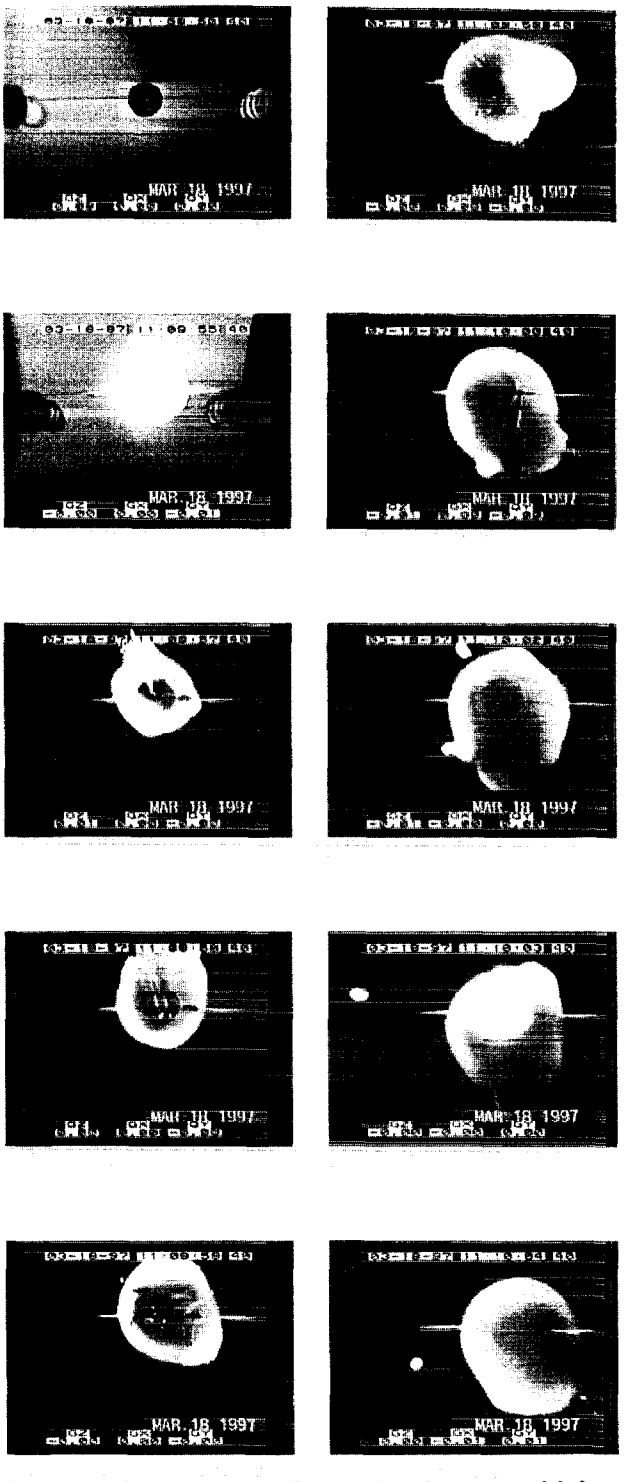

Fig. 4. A video sequence (from top to bottom and left to right) showing a PP sphere before and after ignition under reduced gravity conditions (D_o = 3 mm, 0.10 MPa, and 30% O_2).

of material from the break-up of a bubble jet [33]. The release of gas jets and the ejection of jet particles are clearly shown in Fig. 4. Since the viscosity of the molten polymer depends on its molecular weight [1], the break-up of a

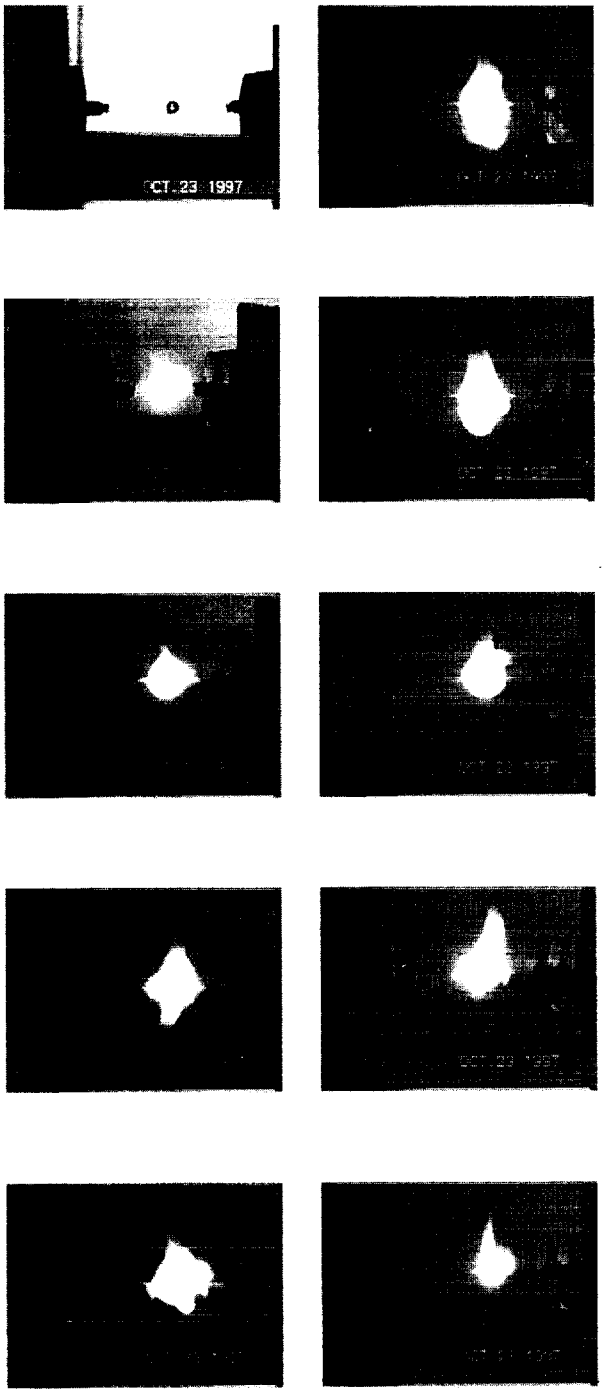

Fig. 5. A video sequence (from top to bottom and left to right) showing a PS sphere before and after ignition under reduced gravity conditions (D_o = 3 mm, 0.05 MPa, and 25% O_2).

bubble jet may be facilitated (in the case of PP) by a less viscous molten layer, a result of random scission of the polymer chain during thermal degradation [34].

The velocities of the ejected material were estimated by tracking the material in two consecutive video frames. An ambiguity arises as to the direction of the ejected material relative to the two-dimensional view provided by the camera. Although two cameras were used, positioned 90° apart, the large number of ejection events precluded identifying individual tracks. Thus, a range of possible velocities was associated with each observation. If, however, the ejection process is assumed to be random with direction, then statistically, the actual velocity (V_a) is related to the measured velocity (V_m) as:

$$V_a = V_m \int_0^{\frac{\pi}{2}} \sec(\theta) d\theta = 1.56 V_m$$

For the PP spheres, V_a = 2.3 (± 1.2) cm/s (with 60 events observed). The ejected material appeared to decelerate at an average rate of ≈ 40 cm/s^2, and traverse an average distance of only ≈ 8 mm before burning to completion. The value of V_a for PMMA and PS was not determined because the ejected material was never observed to exist beyond the visible flame of the parent sphere (see Figs. 2 and 5). However, the presence of ejection events was evident from instantaneous bulges in the visible flame of the (PMMA and PS) parent spheres (and the frequency of material ejection was determined). The average ejection frequency (E_f) is defined here as the number of ejection events divided by the total burning time of the sphere. The ejection frequency measurements did not differentiate between the two types of ejection events. Unlike the velocity, measurement of this parameter does not suffer from ambiguity associated with the two-dimensional view provided by the camera. Once ejection began, the ejection frequency tended to increase over the burning duration. The value of E_f was found to be sensitive to polymer type and independent of pressure. In addition, E_f tended to increase with oxygen concentration although the results are not statistically significant when experimental uncertainty is considered. It should be noted that the change in burn duration as the oxygen concentration varied was small (for example, see Fig. 6 where its value changes ≈15%). The experimental uncertainty (dominated by variance) in the ejection frequency was much larger than this (≈ 30%). The average value of E_f was 3 Hz, 5 Hz, and 5 Hz for all of the PMMA, PS, and PP data, respectively.

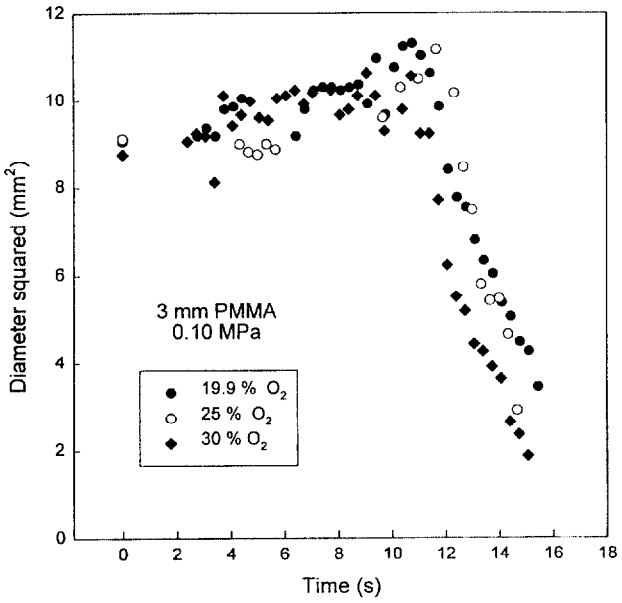

Fig. 6. D^2 vs. time plots for 3-mm PMMA spheres with three oxygen mole fractions of 19.9%, 25%, and 30%, all with initial pressures of 0.10 MPa. The observed duration of the first phase (t_1) was 10.8 s, 11.7 s, and 10.8 s; the time required for complete burning (t_b) was measured as 19.3 s, 16.9 s, and 16.5 s; and the average burning rate constant during phase 2 was 1.3 mm^2/s, 2.1 mm^2/s, and 1.8 mm^2/s for 19.9%, 20%, and 30% ambient oxygen concentration, respectively.

Since the ejection of material and the ejection frequency are likely related to the formation and transport of bubbles in the polymer melt and bubble bursting at the sample surface, the pyrolysis rate may play a role in the ejection events. However, the mechanisms of bubble nucleation, growth, and transport in time-varying temperature and viscosity gradients are so complex, that it is difficult to interpret the ejection events simply based on global condensed-phase kinetics [1].

The diameter of the burning ejected material was obscured by the luminosity of its flame. In addition, an estimate of the diameter of the ejected material based on flame size has a very large uncertainty. It was possible, however, to determine an upper limit estimate of the mass of ejected material based on the observed burning duration of the ejected material (see below). It should be noted that bubble formation occurred at a much greater rate than E_f and that the release of vapor from bubble bursting is not easily estimated.

Burning Rate

Although the condensed-phase processes are complex, previous studies have successfully used the simple D^2-law to analyze results obtained from combustion experiments using polymer spheres in normal gravity [2–4]. The application of the D^2-law, which is an approach used to simplify the treatment of the condensed-phase processes, is based on the observation of an approximately linear relationship between the square of the sphere diameter and time in the experiments. The D^2-law can be written as:

$$D(t)^2 = D_o^2 - Kt \tag{1}$$

where D is the time-dependent sphere diameter, D_o is the initial diameter, K is the burning rate constant, and t is time. This law provides a heuristic explanation for the measurements made in this study. Figure 6 shows representative D^2 vs. time plots for 3-mm-diameter PMMA spheres burning under various initial oxygen concentrations with an initial pressure of 0.10 MPa. These data were extracted from selected high-contrast video images of the time-dependent diameter of the burning spheres. Figure 6 shows that for solid polymer spheres, the apparent burning behavior was characterized by two distinct periods: an initial period when the diameter increased slightly (approximately 10%), and a second final period when the diameter decreased fairly rapidly in a near-linear D^2 manner until complete burning was accomplished.

The apparent diameter of the sphere is due to a competition between diameter reduction due to mass loss from burning and sputtering, and diameter expansion due to the processes of swelling (density decrease with heating) and bubble growth. During the initial period, Fig. 6 shows that the diameter increased only slightly, implying that mass loss was balanced by the expansion processes of swelling and bubbling. In ambient pressure liquid droplet burning, a similar phenomenon associated with initial heating has been identified, when the droplet size hardly changes during a very short initial period [35]. A short heat-up period has also been observed in normal gravity combustion of small (< 2 mm) polymer spheres [4]. In contrast

to the liquid fuel heat-up period, the initial period of diameter expansion is generally very long for the solid fuels and conditions studied here, typically persisting for nearly half of the entire burn duration. For liquid droplet combustion, the slope of a best-fit line through a plot of D^2 versus time, yields a burning rate constant. Because of the ambiguities associated with polymer bubbling and swelling, a time-averaged mass burning rate, determined over the entire combustion period, was used to characterize the polymer combustion.

The time-averaged mass burning rate can be written as:

$$\dot{m}_{ave} = \frac{m_o}{t_b} = K\, m_o\, D_o^{-2} \tag{2}$$

where m_o is the initial polymer mass, D_o is the initial diameter, and t_b is the burning duration. K is the average burning rate constant and is related to D_o and t_b:

$$K = \frac{D_o^2}{t_b} \tag{3}$$

For a sphere, by definition: $m_o = \rho_o\, \pi\, (D_o^3/6)$, where ρ_o is the initial polymer density. For a given initial pressure and oxygen mole fraction (X_o), the time-averaged mass burning rate becomes:

$$\dot{m}_{ave} = \frac{\pi}{6}\, \rho_o\, D_o\, K \tag{4}$$

Because of their impulsive motion and non-spherical flame shape, it was very difficult to obtain accurate measurements of the transient sphere and flame diameters from the video images. However, for a sphere that burns to completion over the reduced gravity period, the average burning rate constant K can be obtained from Eq. 3, using the measured burning duration (t_b). Similarly, the average mass burning rate ($\dot{m}_{ave}$) can be calculated using Eq. 2. The burn duration (t_b) was obtained from the video record using frame-by-frame analysis. Uncertainty in the measurement was less than 30 ms, leading to an uncertainty in the burning rate calculations of less than 2%. The expanded uncertainty (σ) for K was generally less than 10%, with this value dominated by measurement variance. The results are summarized in Table 2, where the average mass burning rate and its uncertainty for PMMA are shown as a function of initial sphere diameter, oxygen concentration, and pressure. The number of runs in the table does not reflect the number of attempts in performing reduced-gravity experiments, but rather indicates the number of successful runs. Some data scatter is evident in the table. For example, the 3-mm, 0.05-MPa results show a decreasing mass burning rate with oxygen concentration. The data scatter was likely due to a number of factors including (1) the low number of runs reported for some conditions; (2) the ejection of material from the polymer melt; and (3) difficulties in controlling the ignition process. For example, slight mispositioning of the polymer spheres could cause preferential contact of the ignition coil with the polymer. Depending on the conditions, the 2-s ignition time was approximately 10% to 20% of the burning time. Unnecessarily prolonged contact of the heating coils with the sample surface may have increased the burning rate. Heat conduction along the suspended wire to the sphere interior may have also played a role, especially near the end of burning. The heat conduction along the support wire can be estimated by $\dot{Q}_{cond} \approx 2k_s\, (T_f - T_s/r_f - r)\, \pi\, R_1^2$, where k_s is the thermal conductivity of the wire, T_f is the flame temperature, T_s is the surface temperature of the sphere, r_f is the flame radius, r is the sphere radius, and R_1 is the radius of the wire. The factor 2 takes into account heat conduction into the sphere from the two directions. With k_s and R_1 fixed and assuming the flame front stand-off ratio $(r_f/r) \approx$ constant and $T_f - T_s \approx$ constant, then $\dot{Q}_{cond} \sim (1/r)$. Therefore, as $r \to 0$, $\dot{Q}_{cond}$ is comparable to $\dot{m}\, L$, where L is the latent heat of gasification. For finite r, however, an order of magnitude estimate shows that $\dot{Q}_{cond} << \dot{m}\, L$.

Despite the data scatter, several trends are apparent in Table 2: (1) the average mass burning rate increased with the initial sphere diameter; (2) the average mass burning rate increased with oxygen concentration; and (3) the average mass burning rate did not seem to be affected significantly by pressure (for the range of pressures studied here). Each of these observations is consistent with Equations 2 and 4. For a given X_O and pressure (K is constant),

TABLE 2

Summary of Average PMMA Burning Rates ($\times 10^4$ g/s) under Various Initial Conditions

D_o (mm)	19.9% O_2	21.0% O_2	25.0% O_2	30.0% O_2
0.05 MPa				
2.0	5.4 ± 0.4[a]	5.8 ± 0.2	7.5 ± 0.5	6.7 ± 0.1
	(N[b] = 3)	(N = 3)	(N = 5)	(N = 3)
2.5	6.4 ± 0.6	7.5	7.8 ± 0.4	7.9 ± 0.8
	(N = 3)	(N = 1)	(N = 5)	(N = 3)
3.0	11.5	10.2 ± 3.9	8.99 ± 0.50	9.66 ± 0.18
	(N = 1)	(N = 2)	(N = 4)	(N = 3)
0.10 MPa				
2.0	5.4 ± 0.4	5.9 ± 0.6	6.4 ± 0.6	7.2 ± 0.2
	(N = 3)	(N = 5)	(N = 4)	(N = 3)
2.5	7.1 ± 0.3	7.4 ± 0.5	7.3 ± 0.1	8.8 ± 0.4
	(N = 3)	(N = 5)	(N = 3)	(N = 3)
3.0	8.2	8.6 ± 0.7	9.4 ± 0.9	10.2 ± 0.6
	(N = 1)	(N = 3)	(N = 3)	(N = 3)
0.15 MPa				
2.0	6.2 ± 0.4	5.6 ± 0.1	6.8 ± 0.8	6.9 ± 0.6
	(N = 2)	(N = 2)	(N = 2)	(N = 3)
2.5	6.5	7.3 ± 0.2	7.6 ± 0.3	8.4 ± 0.6
	(N = 1)	(N = 2)	(N = 2)	(N = 3)
3.0	7.7	8.5 ± 0.01	9.1 ± 0.6	10.0 ± 0.5
	(N = 1)	(N = 2)	(N = 2)	(N = 3)

[a] Mean ± standard deviation.
[b] Number of runs.

$\dot{m}_{ave} \sim D_o$. For a given D_o and pressure, $\dot{m}_{ave}$ increases with X_O because K increases with X_O. For given D_o and X_O, $\dot{m}_{ave}$ is relatively independent of the pressure because K is not sensitive to the range of pressures used here. The average mass burning rate of the PS spheres was also found to be proportional to the initial sphere diameter in normal gravity combustion studies [9].

Figure 7 shows the values of the average K and its standard deviation (σ) as a function of the initial oxygen concentration. Average values of K were determined using Eq. 3 and the data in Table 2. Since the average K does not significantly vary with pressure and D_o, all of the data in Table 2 were used to plot Fig. 7. Also shown in Fig. 7 are K values estimated using the B number [35]. The B number was calculated using an average flame temperature for the thermophysical properties, as recommended by Law [35]. This temperature (≈ 1400 K) represents an average of the adiabatic flame temperature (2200 K) and the polymer surface temperature (≈ 640 K), measured in normal gravity [36]. As X_O varies, the B number takes values such that: $1 < B < 2$. Figure 7 shows that the relative trends in the reduced gravity PMMA burning rate measurements compare favorably to the trends estimated using the B number, although the absolute values differed by as much as 50%.

Only a limited number of experiments were performed using PP and PS. Table 3 compares the average mass burning rate of PP and PS with

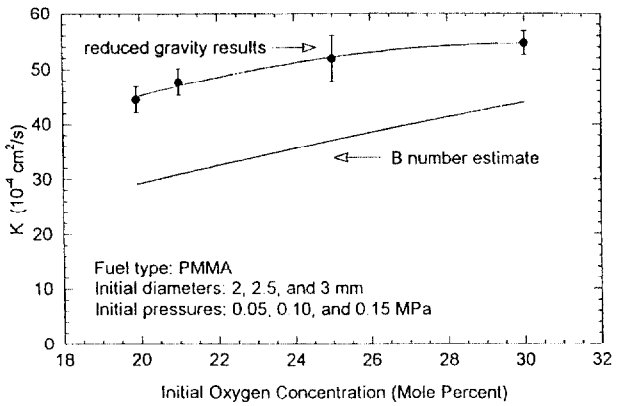

Fig. 7. The average K and its standard deviation (σ) as a function of the initial oxygen concentration. Also shown are estimated K values using the B number.

TABLE 3

Comparison of Average Burning Rates for Different Thermoplastics and Initial Conditions

Material	D_o (mm)	Oxygen (%)	Pressure (MPa)	N^a	$(\dot{m}_{ave} \pm \sigma)^b \cdot 10^4$ (g/s)
PMMA	3.0	30	0.10	3	10.2 ± 0.6
PP	3.0	30	0.10	2	7.0 ± 0.5
PMMA	3.0	25	0.10	3	9.4 ± 0.9
PP	3.0	25	0.10	1	5.81
PMMA	3.0	25	0.05	5	9.0 ± 0.5
PS	3.0	25	0.05	4	8.7 ± 0.8

[a] Number of runs.
[b] Mean ± standard deviation.

those of PMMA for the same experimental conditions. The dependence of mass burning rate on oxygen concentration is also evident for PP spheres. The average mass burning rate of PMMA is significantly higher than that of PP and is similar to that of PS.

An upper limit estimate of the mass of ejected material for PP can be determined using Eq. 3, and assuming that the ejected material is condensed-phase and that its density, $\rho_e \approx 1$ g/cm^3 [37]. Using K from Table 3, the mass of ejected material (m_e) can be estimated as $\approx (4/3)\pi\rho_e(D_e/2)^3$, where D_e ($= \sqrt{K\, t_{be}}$) is the diameter of the ejected material and t_{be} is the observed duration of the burning of the ejected material. The total contribution to the burning rate for the ejected material is the product of the frequency of ejection (E_f) and the average mass for each ejection, $E_f\, m_e \approx 10^{-5}$ g/s (± 50%) for PP (at 25% O_2), which represents a small ($\approx 1\%$) contribution to the overall burning rate. The large uncertainty is associated with the video framing rate and the short burning duration of the ejected material ($t_{be} \approx 2$ frames or 0.07 s). The contribution to the overall mass burning rate for ejections in the PMMA and PS spheres is smaller, if the ejections are due solely to the release of gaseous material.

Estimate of the Void Fraction of the Polymer Sphere

As the polymer sphere heats up, the processes of bubble nucleation and growth are responsible for the existence of gas-phase polymer degradation products that form a significant fraction of the sphere volume. The gas-phase void fraction of the burning polymer sphere was estimated by considering the sphere as a homogeneous two-phase mixture. Competing with the bubble formation processes are losses due to bubble release and evaporation from the polymer surface. The mass burning rate, $\dot{m}$, can be written as:

$$\dot{m} = -\frac{d}{dt}\left[\frac{4\pi}{3}\rho_d\left(\frac{D}{2}\right)^3\right] \tag{5}$$

If the sphere is composed of bubbles of average density ρ_v and a solid melt of average density ρ_m and the sphere contains a time-varying void volume fraction, $\alpha(t)$, then the sphere density (ρ_d) is:

$$\rho_d = \alpha\rho_v + (1 - \alpha)\rho_m \tag{6}$$

In Eq. 6, it is implicitly assumed that the solid sphere has reached a molten state upon ignition. This assumption is reasonable because a simple moving-boundary heat conduction calculation indicates that the melting front has almost penetrated to the center of the sphere within 2 seconds. Substituting Eq. 6 into Eq. 5:

$$-\frac{6\dot{m}}{\pi D^3} = -(\rho_m - \rho_v)\frac{d\alpha}{dt} + \frac{3}{D}\frac{dD}{dt}\rho_d \tag{7}$$

where the apparent diameter is controlled by the time-averaged mass loss and the transient void fraction.

As mentioned previously, the experimental results (e.g., Fig. 6) indicate that two distinct phases exist during burning of the polymer spheres. During the initial phase, the diameter is relatively constant, and during the second phase the square of the diameter linearly decreases with time until the sphere burns to completion at time t_b:

$dD/dt \approx 0$ and $D \approx D_o$

$$\text{for } 0 \le t \le t_1 \text{ (phase 1)} \tag{8}$$

$$D^2 = D^2(t = t_1) - K_2(t - t_1)$$

$$\text{for } t_1 \le t \le t_b \text{ (phase 2)} \tag{9}$$

During phase 2, K_2 is the average burning rate constant. If $t_1 = 0$, then $K_2 = K$ (where K is the average burning rate constant over t_b as defined in Eq. 1). The initial condition for the diameter during phase 2 is: $D(t = t_1) \approx D_o$.

Applying the phase 1 conditions (Eq. 8) to the governing equation (Eq. 7) and assuming that the mass burning rate is constant ($\dot{m} \approx$ constant) and that the void fraction is initially zero ($\alpha = 0$ at $t = 0$), obtains:

$$\alpha = \frac{6\dot{m}_{ave}\, t}{\pi D_o^3(\rho_m - \rho_v)} \qquad 0 \le t \le t_1 \tag{10}$$

The assumption of constant $\dot{m}$ is reasonable because in combustion experiments at normal gravity using PMMA and PS spheres, mass loss was observed to decrease linearly with time for a significant portion of the total burning time [3, 4].

At the end of phase 1, Eq. 10 shows that:

$$\alpha(t = t_1) \equiv \alpha_1 = \frac{6\dot{m}_{ave}\, t_1}{\pi D_o^3(\rho_m - \rho_v)} \tag{11}$$

To evaluate α during phase 2, the derivative of the D^2-law is determined:

$$\frac{dD}{dt} = \frac{1}{2}\frac{-K_2}{\sqrt{D_o^2 - K_2(t - t_1)}} \tag{12}$$

Introducing Eqs. 6 and 12 into Eq. 7, yields a first-order differential equation in terms of α:

$$\frac{d\alpha}{dt} = \frac{3}{2}\frac{K_2\alpha}{[D_o^2 - K_2(t - t_1)]} + \frac{6\dot{m}_{ave}}{\pi(\rho_m - \rho_v)[D_o^2 - K_2(t - t_1)]^{3/2}} - \frac{3K_2\rho_m}{2[D_o^2 - K_2(t - t_1)](\rho_m - \rho_v)} \tag{13}$$

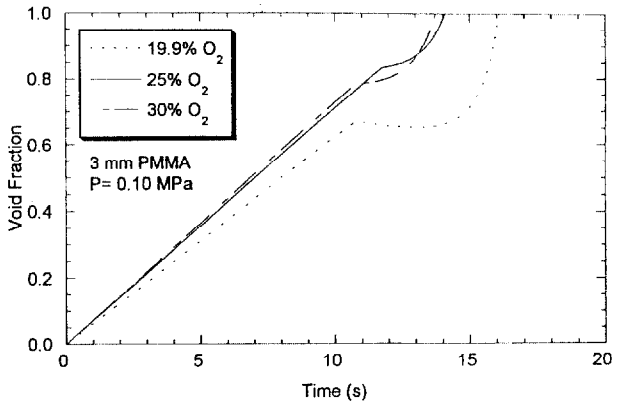

Fig. 8. The calculated void volume fraction (α) corresponding to the data shown in Fig. 6.

Integrating this relation and imposing the conditions (at $t = t_1$) defined by Eqs. 9 and 11 yields the solution for α during phase 2 ($t_1 \le t \le t_b$):

$$\alpha = \frac{6\dot{m}_{ave}t}{\pi(\rho_m - \rho_v)[D_o^2 - K_2(t - t_1)]^{3/2}} + \frac{\rho_m}{(\rho_m - \rho_v)} \cdot \left\{1 - \frac{D_o^3}{[D_o^2 - K_2(t - t_1)]^{3/2}}\right\} \tag{14}$$

where t_1 (and thereby α_1 through Eq. 11) are empirically determined. The average PMMA melt density (ρ_m) for temperatures between ambient and 400 K was taken from Ref. 38. A linear extrapolation of that data was used for temperatures greater than 400 K. A polynomial fit to that data yields:

$$\rho_m(\text{g/cm}^3) = 1.2042 - 5.0434 \times 10^{-4}T - 1.0437 \times 10^{-7}T^2$$

where T is in Celsius. The vapor-phase density is assumed to be much smaller than the melt density, (i.e., $\rho_v << \rho_m$).

Figure 8 shows the calculated void fraction (α) as a function of time from Eqs. 10 and 14 for the experiments corresponding to those shown in Fig. 6, for 3 mm PMMA spheres with X_O = 19.9%, 25.0%, and 30.0%. The PMMA density (ρ_m) was taken as 1 g/cm^3 in the calculation, which represents an average polymer melt temperature of 670 K. A sensitivity analysis showed that α is not strongly affected by changes in the melt density.

Figure 8 shows that bubbles are a significant, if not dominant fraction of the sphere volume over most of the burning duration. The calculation results suggest that the void fraction increases with time, with between 60% to 80% of the sphere volume attributable to bubbles at t_1. In phase 2, the void fraction first levels off, and then rapidly increases until $\alpha = 1$. The time when $\alpha = 1$ can be interpreted as the burn-out time (t_b), when the melt has been completely vaporized. Figure 8 shows that the model predicts that t_b is equal to 16.0 s, 14.1 s, and 13.7 s for the data corresponding to that shown in Fig. 6 with $X_O = 19.9\%$, 25.0%, and 30.0%, respectively. The calculated values of t_b are 2.8 s to 3.3 s shorter than the measured values, indicating the limitations of this simple homogeneous two-phase model (see Fig. 6). Still, the calculated results lend semiquantitative insight into bubble behavior during the burning of a solid thermoplastic. The large value of the void fraction suggests that the mass loss mechanism associated with the escape of bubbles from the surface of the sphere may play a significant role in the burning rate (especially late into the burn), perhaps even superseding mass loss due to evaporation at the polymer surface. Unfortunately, it was not possible to differentiate mass loss due to bubble bursting from vaporization at the sphere surface. Measurement of the transient void fraction would guide refinement of the model. Such measurements are very challenging and remain to be accomplished.

CONCLUSIONS

The low-gravity combustion experiments of thermoplastic (PMMA, PP, and PS) spheres reveal several interesting phenomena, which are not observed in normal gravity. Whereas dripping of a polymer melt can pose a fire hazard in normal gravity, in the case of PP, the random and violent ejection of burning material in microgravity represents a nontrivial fire safety challenge. The three thermoplastic types used in the reduced gravity experiments exhibited very different combustion characteristics. The two types of bubble bursting phenomena, the release of a gas jet and the ejection of condensed-phase material from the break-up of a bubble jet, offer a plausible explanation for the dynamic ejection events during combustion of the three types of polymers studied here. The average mass burning rates of PMMA were found to increase with the initial sphere diameter and oxygen concentration and were not affected significantly by pressure. Under the same initial conditions, the average mass burning rate of PP was lower than PMMA, whereas the mass burning rate of PS was similar to PMMA.

Calculations show that during burning, a large fraction of the sphere is composed of gaseous bubbles that nucleate, grow and escape from the polymer, causing sputtering of molten burning solid polymer. Unlike liquid droplets, diameter expansion of the molten fuel occurs mainly due to the in-depth formation and growth of bubbles, whereas the decreased density accompanying polymer heating also contributes. Sputtering and the escape of bubbles from the sphere surface acts to enhance the mass loss rate of polymer burning.

Based on our observations of the suspended burning polymer spheres, experiments burning unsupported thermoplastic spheres are likely not feasible, because of the impulsive motion caused by the sputtering and ejection of molten material, which will cause an unsupported sphere to drift from the field of view of a video recorder.

This work is supported by NASA Lewis Research Center under NASA Interagency Agreement C-32017-C. The authors would like to thank Mr. Roy McLane for performing some of the parabolic flight experiments, the staff at the NASA-LeRC Reduced Gravity Aircraft Facility and the NASA-JSC KC-135 Office for their technical assistance in the parabolic flight experiments, Dr. Howard Ross of LeRC, Dr. Liming Zhou of SAIC, Drs. Takashi Kashiwagi and Kathryn Butler of NIST for many stimulating discussions, Ms. Nikki Privé of NIST for analyzing data, and Prof. Seung Baek, a NIST Guest Researcher from the Korea Advanced Institute of Science and Technology for reading the first draft of the manuscript and for providing many useful comments. This paper is dedicated to the memory of Mr. Michael Glover of NIST who fabricated many of the experimental components and who enthusiastically performed several of the parabolic flight experiments.

REFERENCES

1. Kashiwagi, T., *Twenty-Fifth Symposium (International) on Combustion*, The Combustion Institute, Pittsburgh, 1994, pp. 1423–1437.
2. Essenhigh, R. H., and Dreier, W. L., *Fuel* 48:330–342 (1969).
3. Waibel, R. T., and Essenhigh, R. H., *Fourteenth Symposium (International) on Combustion*, The Combustion Institute, Pittsburgh, 1973, pp. 1413–1420.
4. Raghunandan, B. N., and Mukunda, H. S., *Fuel* 56: 271–276 (1977).
5. Wendt, J. O., *Prog. Energy Combust. Sci.* 6:201–222 (1980).
6. Chung, S. L., and Tsang, S. M., *J. Air Waste Manage. Assoc.* 41:821–826 (1991).
7. Chung, S. L., and Lai, N. L., *J. Air Waste Manage. Assoc.* 42:1082–1088 (1992).
8. Panagiotou, T., and Levendis, Y., *Combust. Flame* 99:53–74 (1994).
9. Panagiotou, T., Levendis, Y., and Delichatsios, M. A., *Combust. Sci. Technol.* 103:63–84 (1994).
10. Panagiotou, T. and Levendis, Y., *Combust. Sci. Technol.* 112:117–140 (1996).
11. Panagiotou, T., Levendis, Y., Carlson, J., and Vouros, P., *Twenty-Sixth Symposium (International) on Combustion*, The Combustion Institute, Pittsburgh, 1996, pp. 2421–2430.
12. Panagiotou, T., Levendis, Y., Carlson, J., Dunayevskiy, Y. M., and Vouros, P., *Combust. Sci. Technol.* 116:91–128 (1996).
13. Aseeva, R.M., and Zaikov, G.E., *Combustion of Polymeric Materials*, Hanser Publishers, Munich, 1981.
14. Melikhov, A. S., Potyakin, V. I., Ryzhov, A. M., and Ivanov, B. A., *Combust. Explos. Shock Waves* 19:393–395 (1983).
15. Goldmeer, J. S., Urban, D. L., and T'ien, J. S., *Eastern States Section of the Combustion Institute, Fall Technical Meeting*, Princeton University, Princeton, NJ, Oct. 25–27, 1993, pp. 441–444.
16. Olson, S. L., and Hegde, U., *Eastern States Section of the Combustion Institute, Fall Technical Meeting*, Clearwater Beach, FL, Dec. 5–7, 1994, pp.348–351.
17. Goldmeer, J. S., T'ien, J. S., and Urban, D. L., *Fourth International Microgravity Combustion Workshop*, Cleveland, May 19–21, 1997, pp. 435–440.
18. Williams, F. A., *Combustion Theory*, Benjamin-Cummings, Menlo Park, CA, 1985.
19. Yang, J. C., and Hamins, A., *Third International Microgravity Combustion Workshop*, Cleveland, April 11–13, 1995, pp. 115–120.
20. Yang, J. C., Hamins, A., Glover, M., and King, M. D., *Fourth International Microgravity Combustion Workshop*, Cleveland, May 19–21, 1997, pp. 243–248.
21. Okajima, S., Kawakami, T., and Raghunandan, B. N., Work-in-Progress Poster Session, *Twenty-Sixth Symposium (International) on Combustion*, The Combustion Institute, Pittsburgh, 1996.
22. Okuyama, Y., Ohtomo, Y., Maruta, K., Kobayashi, H., and Niioka, T., *Twenty-Sixth Symposium (International) on Combustion*, The Combustion Institute, Pittsburgh, 1996, pp. 1369–1375.
23. Wichman, I. S., *Combust. Flame* 63:217–229 (1986).
24. Butler, K. M., *Fourth International Microgravity Combustion Workshop*, Cleveland, May 19–21, 1997, pp. 249–254.
25. Mikami, M., Kono, M., Sato, J., Dietrich, D. L., and Williams, F. A., *Combust. Sci. Technol.*, 90:111–123 (1993).
26. Vieille, B., Chauveau, C., Chesneau, X., Odeïde, A., and Gökalp, I., *Twenty-Sixth Symposium (International) on Combustion*, The Combustion Institute, Pittsburgh, 1996, pp. 1259–1265.
27. Seshadri, K., and Williams, F. A., *J. Polymer Sci.* 16:1755–1778, (1978).
28. Tewarson, A., *A Smoke Point Height and Fire Properties of Materials*, NIST-GCR-88-555, U.S. Department of Commerce, Washington, D.C., 1988.
29. Hara, H., and Kumagai, S., *Twenty-Third Symposium (International) on Combustion*, The Combustion Institute, Pittsburgh, 1990, pp. 1605–1610.
30. Jackson, G. S., Avedisian, C. T., and Yang, J. C., *Int. J. Heat Mass Transfer* 35:2017–2033 (1992).
31. Jackson, G. S., and Avedisian, C. T., *Proc. Roy. Soc. London* A 446:255–276 (1994).
32. Avedisian C. T., Yang, J. C., and Wang, C. H., *Proc. Roy. Soc. London* A 420:183–200 (1988).
33. Tomaides, M., and Whitby, K. T., in *Fine Particles, Aerosol Generation, Measurement, Sampling, and Analysis* (B. Y. H. Liu, Ed.), Academic Press, New York, 1976.
34. Cullis, C. F., and Hirschler, M. M., *The Combustion of Organic Polymers*, Clarendon Press, Oxford, 1981.
35. Law, C. K., *Prog. Energy Combust. Sci.* 8:171–201 (1982).
36. Vovelle, C., Delfau, J. L., Reuillon, M., Bransier, Q., and Laraqui, N., *Combust Sci Technol.* 53:187–201 (1987).
37. Troitzsch, J., *International Plastics Flammability Handbook, Principles–Regulations–Testing and Approval*, Macmillan, New York, 1983.
38. Wittmann, J. C., and Kovacs, A. J., *J. Polymer Sci.*, Part C, 16:4443–4452 (1969).

Received 15 September 1998; revised 26 April 1999; accepted 25 May 1999